AGU PUBLICATIONS

JGR

Journal of Geophysical Research: Earth Surface

RESEARCH ARTICLE
10.1002/2016JF003926

Key Points:
- An optimal average density of 750 kg/m^3 is the first time estimated in Alaska
- The ice mass loss in Alaska is estimated with -57.5 Gt from ICESat measurements
- The GIA uplift rates and the best fitting model are estimated in Alaska

Correspondence to:
S. Jin,
sgjin@shao.ac.cn;
sg.jin@yahoo.com

Citation:
Jin, S., T. Y. Zhang, and F. Zou (2017), Glacial density and GIA in Alaska estimated from ICESat, GPS and GRACE measurements, *J. Geophys. Res. Earth Surf.*, *122*, 76–90, doi:10.1002/2016JF003926.

Received 19 APR 2016
Accepted 15 DEC 2016
Accepted article online 19 DEC 2016
Published online 10 JAN 2017

Glacial density and GIA in Alaska estimated from ICESat, GPS and GRACE measurements

Shuanggen Jin[1], T. Y. Zhang[1,2], and F. Zou[1]

[1]Shanghai Astronomical Observatory, Chinese Academy of Sciences, Shanghai, China, [2]University of Chinese Academy of Sciences, Beijing, China

Abstract The density of glacial volume change in Alaska is a key factor in estimating the glacier mass loss from altimetry observations. However, the density of Alaskan glaciers has large uncertainty due to the lack of in situ measurements. In this paper, using the measurements of Ice, Cloud, and land Elevation Satellite (ICESat), Global Positioning System (GPS), and Gravity Recovery and Climate Experiment (GRACE) from 2003 to 2009, an optimal density of glacial volume change with 750 kg/m^3 is estimated for the first time to fit the measurements. The glacier mass loss is -57.5 ± 6.5 Gt by converting the volumetric change from ICESat with the estimated density 750 kg/m^3. Based on the empirical relation, the depth-density profiles are constructed, which show glacial density variation information with depths in Alaska. By separating the glacier mass loss from glacial isostatic adjustment (GIA) effects in GPS uplift rates and GRACE total water storage trends, the GIA uplift rates are estimated in Alaska. The best fitting model consists of a 60 km elastic lithosphere and 110 km thick asthenosphere with a viscosity of 2.0×10^{19} Pa s over a two-layer mantle.

1. Introduction

The mountains around the Gulf of Alaska are covered by some of the largest glaciers on the Earth excluding the polar ice sheets over Antarctica and Greenland. It has been reported that the mountain glaciers in Alaska are melting rapidly due to the recent climatic change, which greatly contribute to the global sea level rise [*Larsen et al*., 2007; *Jin and Feng*, 2016]. Due to the limited and high-cost traditional observations of the glaciers, it is difficult to quantify the glacier melting in Alaska. The Gravity Recovery and Climate Experiment (GRACE) mission, jointly sponsored by the National Aeronautics and Space Administration (NASA) and the German Aerospace Center (DLR), has provided a unique opportunity to estimate the mass change on the Earth's surface [*Tapley et al*., 2004; *Jin et al*., 2011, 2012]. The mass changes of Greenland [*Velicogna and Wahr*, 2005] and Antarctic glacier ice sheets have been successfully estimated by GRACE [*Rignot et al*., 2011; *Velicogna et al*., 2014], which provided a direct view of polar ice melting. Some studies have also been made to assess the ice mass loss on the Alaskan glaciers [*Chen et al*., 2006; *Luthcke et al*., 2008; *Beamer et al*., 2016]. However, the glacial isostatic adjustment (GIA) effects not only from the Last Glacial Maximum (LGM) but also viscous component of post-Little Ice Age (LIA) isostatic adjustments have existed on the Alaskan Mountains [*Larsen et al*., 2005; *Sato et al*., 2011]. The imprecise glacial isostatic adjustment (GIA) effects result in large uncertainty in estimating the ice mass loss trend in Alaska from GRACE.

Another space geodetic technique, laser altimetry can also measure the glacier change. The repeated airborne altimeter measurements can estimate the regional mass balance [*Larsen et al*., 2015] but have low temporal-spatial resolution. The Ice, Cloud, and land Elevation Satellite (ICESat) mission has been launched in 2003 to measure the surface elevation change of the glaciers. The satellite altimeter onboard ICESat has provided the measurements on the global scale, which can be used to estimate the ice volume loss [*Howat et al*., 2008]. The ice mass loss estimation from ice volume loss depends on the assumption of the density of glacial volume change, which is referred to the portion gained or lost from the system. The density of glacial volume change is greatly affected by the uncertainty associated with snow and firn densification [*Huss*, 2013], depending on things like snow/firn temperature and the presence or absence of liquid water. Sorge's law is defined by the assumption of a constant surface accumulation rate, so any deviation from that creates uncertainty. In addition, things like rain-on-snow events also dramatically alter the near surface density profile. Due to the lack of in situ measurements for the density of Alaskan glaciers, it is difficult to accurately estimate optimal density. By assuming the average density of 900 kg/m^3 based on the Sorge's law [*Bader*, 1954], the

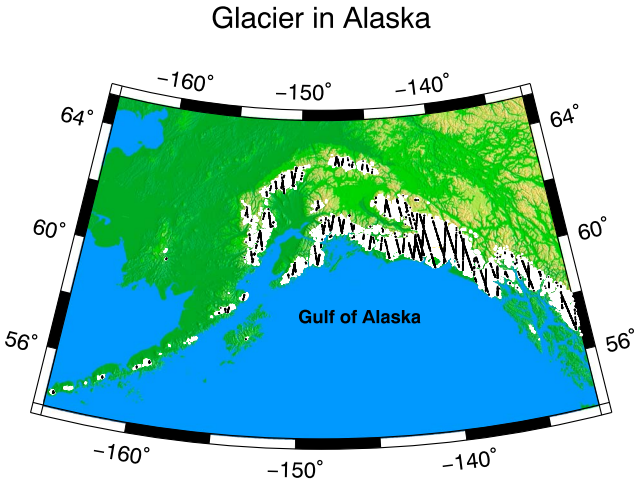

Figure 1. The distribution of glaciers and ICESat measurements in Alaska from 2003 to 2009. The white shading indicates the locations of glaciers from a global glacier inventory [*Arendt et al.*, 2012]. The black dots show the locations of ICESat measurements on the glaciers.

estimated ice mass loss in Alaska was −65 Gt/yr [*Arendt et al.*, 2013]. If the average density is assumed to be 800 kg/m^3, the mass loss of Alaskan glaciers would reduce to be −58 Gt/yr. Therefore, it has large uncertainty of estimating ice mass loss in Alaska from ICESat.

GPS geodetic measurements have become an increasing useful tool to measure the GIA effects from viscoelastic response of the Earth [*Milne et al.*, 2001; *Hu and Freymueller*, 2012] and displacement deformation [*Jin and Park*, 2006; *Jiang et al.*, 2010; *Compton et al.*, 2015; *Avsar et al.*, 2016]. Accelerating uplift measured by GPS stations has been confirmed by the rapid acceleration of ice mass loss [*Bevis et al.*, 2012; *Yang et al.*, 2013; *Bevis and Brown*, 2014]. However, separating the viscoelastic response of the past glacial advance and retreat with elastic response of the modern ice mass loss is challenging without other independent measurements. *Velicogna and Wahr* [2002] proposed and demonstrated to separate GIA effects with ice mass balance signal by using ICESat, GRACE, and GPS data in Antarctica. Due to the sparse GPS stations, it seems impossible to constrain the GIA effects by the limited GPS measurements in Alaska.

In this paper, it is aimed to estimate the optimal average density of the Alaskan glaciers by using ICESat, GRACE, and GPS data. The GIA effects will be modeled by an optimal Earth's model to fit the measurements. This paper is organized as follows: the processing of ICESat, GPS, and GRACE data is introduced in section 2; the results from ICESat, GPS, and GRACE observations are shown in section 3; in section 4 an optimal average density of Alaskan glaciers is estimated to separate the GIA effects with glacier mass loss signals by combining ICESat with GPS and GRACE results, and finally conclusions are given in section 5.

2. Data and Processing

2.1. ICESat Data

If ICESat delivers data on mountain glaciers, it measures the elevation change of the mountain glaciers. The data were acquired along the same ground tracks with a 33 day subcycle of the 91 day repeated orbit. The footprints of the satellite altimetry have a diameter of 70 m and are spaced at about 170 m along the track. This study used the Level-2 Global Land Surface Altimetry Data product-GLA14 of Release 634 [*Zwally et al.*, 2002] provided by the National Snow and Ice Data Center. The corrected surface ellipsoidal heights referenced to the TOPEX/Poseidon ellipsoid are derived from GLA14 products. The products have been corrected by range correction of the troposphere, solid Earth tide, ocean tide, and pole tide. The saturation correction has also taken into account for the delay of the pulse center in saturated returns. The accuracy of ICESat elevation measurement can be better than 0.15 m over gently sloping terrains [*Zwally et al.*, 2002] and 0.05 m in case of no cloud cover [*Shuman et al.*, 2006]. The bias in ICESat elevations resulting from an incorrect selection of the centroid, rather than the Gaussian peak, of the transmit pulse to calculate surface elevation [*Borsa et al.*, 2013] has been corrected in Release 634 products. Figure 1 shows the distribution of glaciers and ICESat measurements in Alaska.

For better comparison with other results, the ellipsoid height of GLA14 is converted to the orthometric height with the reference ellipsoid of WGS84 Ellipsoid and EGM96 Geoid with the following formula [*Ke et al.*, 2015]:

$$h_{\mathrm{hgt}} = h_{\mathrm{elev}} - h_{\mathrm{geoid}} - 0.7 \quad (1)$$

where h_{hgt} is the orthometric height, h_{geoid} is the EGM96 geoid height referred to WGS 84 Ellipsoid at the

location of the footprint and h_{elev} is the height products of GLA14. There is an offset of 0.7 m between the vertical difference between WGS84 Ellipsoid and TOPEX/POSEIDON Ellipsoid [*Bhang et al*., 2007], which is taken into account here. Then the elevation change rates can be obtained by the surface plane fitting method [*Moholdt et al*., 2010; *Moholdt et al*., 2012]. Along each reference track, we fit the multitemporal track points into a rectangular plane with a length of 700 m, which are overlapped by 350 m in each adjacent plane for more observations. The width of the planes was determined by the distance of the repeated profiles, typically a few hundred meters. The elevation change rate for each plane can be estimated by the least squares fitting as the following equation:

$$\begin{bmatrix} dh_1 \\ dh_2 \\ \vdots \\ dh_n \end{bmatrix} = \begin{bmatrix} dE_1 & dN_1 & dt_1 \\ dE_2 & dN_2 & dt_2 \\ \vdots & \vdots & \vdots \\ dE_n & dN_n & dt_n \end{bmatrix} \cdot \begin{bmatrix} S_e \\ S_n \\ dh/dt \end{bmatrix} + \begin{bmatrix} r_1 \\ r_2 \\ \vdots \\ r_n \end{bmatrix} \tag{2}$$

where *dE*, *dN*, *dh*, and *dt* are the differences in position and time (in decimal years) between each point and the average of all points in the plane; S_e and S_n are the slopes in the east and north direction; *dh*/*dt* is the elevation change rate of the plane; and *r* is the residual that contains the remaining elevation variations. In order to obtain a valid estimate of the elevation change rate, the potential outlier points with $r > 10$ m are removed and the regression will be recomputed iteratively when all residuals are less than the threshold. Moreover, all the planes consist of more than 12 track points, four repeated profiles, and longer than 2 year observation time span to insure a robust estimate.

For the entire period of 2003 to 2009, more than 6000 planes (Figure 1) with constant elevation change rates are estimated in this paper, which are still not sufficient for the estimate of the whole Alaskan glacier change. The glacier change rates of the remaining area will be extrapolated by the observations through the hypsometric approach [*Moholdt et al*., 2010].

2.2. GPS Observations

It is almost 20 years since the GPS sites were built to measure the crustal deformation in Alaska. In order to obtain more stable and precise results for geophysical and geodynamic interpretation, a complete reprocessing of GPS data has been developed recently. The precise coordinates can be estimated by GPS with an accuracy of millimeter level for better interpretation of the geophysical and geodynamic process. Here the daily solutions of all 101 continuous GPS stations in Alaska are used from the Jet Propulsion Laboratory, and most observations are from 1997 to 2015.

Because the horizontal velocity of GPS measurements is mostly caused by the plate tectonic motion [*Jin and Park*, 2006], only vertical displacement time series are used in this study. The vertical surface displacement of GPS is sensitive to the variation of the loadings, including the atmospheric and hydrological loadings [*Fu et al*., 2012]. Here the atmospheric loading was removed from the GPS coordinate time series so as to study the loading deformation caused by the hydrological cycle. Here the atmospheric loadings are removed by using the global surface displacement with the resolution of 2.5° from National Centers for Environmental Prediction (http://geophy.uni.lu/ncep-loading.html) [*Van Dam*, 2010]. Before estimating the trend of vertical GPS time series, the coseismic and postseismic effects are removed. Then the vertical GPS time series will be fit as follows:

$$h(t) = A_a \sin(\omega_a t - \varphi_a) + A_{sa} \sin(\omega_{sa} t - \varphi_{sa}) + vt + \Delta h(t) + B + \varepsilon \tag{3}$$

where $h(t)$ are vertical GPS coordinate time series; A_a and A_{sa} are annual amplitude and semiannual amplitude; ϕ_a and ϕ_{sa} are annual phase and semiannual phase, respectively; ω_a and ω_{sa} are the frequency of annual and semiannual terms, as $\omega_a = 2$*pi and $\omega_{sa} = 4$*pi, respectively; *v* is the linear rate of the long-term variations; $\Delta h(t)$ is coseismic and post-seismic deformation by parametric models with the exponential function; *B* is constant; and $\varepsilon(t)$ is the residual error. The linear trend of GPS station time series contains different signals due to tectonic deformation, hydrological loading, and GIA [*Argus et al*., 2005].

To construct a better coverage of GPS stations in Alaskan glacier area, the 55 vertical GPS velocities provided in *Marechal et al*. [2015] are also used here as a supplement. The distribution of all used GPS sitations is shown in Figure 2.

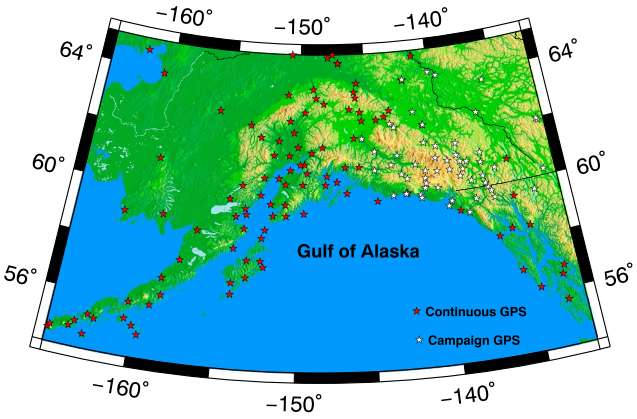

Figure 2. GPS stations in Alaska. The red stars are the continuous GPS stations used in study, and the white stars are the GPS measurements from *Marechal et al*. [2015].

2.3. GRACE Measurements

The Gravity Recovery and Climate Experiment (GRACE) mission with more than 13 year observations provides a unique opportunity to estimate global mass redistribution within the Earth system and hydrological loading [e.g., *Jin et al*., 2013; *Zhou et al*., 2016; *Hassan and Jin*, 2016]. Here we employed the level 2 monthly spherical harmonic coefficients of GRACE Release 05 from the University of Texas at Austin Center for Space Research with a truncation of up to degree 60. The monthly gravity coefficients are provided by Center for Space Research from April 2002 to present (ftp://podaac-ftp.jpl.nasa.gov/allData/grace/L2/CSR/RL05/). The total water storage (TWS) changes are estimated from the monthly GRACE gravity coefficients from April 2002 to December 2014. Some missing month data are interpolated from the adjacent 2 months. The degree 1 gravity coefficients are used from *Swenson et al*. [2008], and the C_{20} component is replaced by the result from Satellite Laser Ranging data [*Cheng and Tapley*, 2004]. The residual stoke coefficients are obtained after removing the mean gravity field for 2003–2014. The processing strategy includes decorrelation destriping, smoothing, and filtering, which can be found in previous studies [*Wahr et al*., 2004; *Swenson and Wahr*, 2006; *Jin and Feng*, 2013]. In order to reduce the systematic and correlated errors of GRACE measurements, the 300 km width of Gaussian filter and destriping filter [*Swenson and Wahr*, 2006] are applied to the GRACE observations. The mass anomalies are usually expressed as equivalent water thickness from the following equation:

$$\Delta H(\phi,\lambda) = \frac{R_e \rho_e}{3\rho_w} \sum_{n=0}^{60} \sum_{m=0}^{n} \frac{(2n+1)}{1+k_n} W_n P_{nm}(\sin\phi)\left\{\Delta \bar{C}_{nm} \cos m\lambda + \Delta \bar{S} \sin m\lambda\right\} \tag{4}$$

where $W_n = \exp\left[-\frac{(nr/R_e)^2}{4\ln(2)}\right]$ is the Gaussian filter; R_e and ρ_e are the mean equatorial radius and average density of the Earth; ρ_w is the density of fresh water; ϕ and λ are the geographic latitude and longitude; P_{nm} are the fully normalized Associated Legendre Polynomials of degree n and order m; r is the Gaussian averaging radius; k_n is the load Love number of degree n; and $\Delta \bar{C}_{nm}$, $\Delta \bar{S}$ are the residual stoke coefficients. The gravity coefficients are converted into grid TWS with a resolution of 1°.

To be consistent with GPS processing strategy, the equivalent water thickness is determined by the approach of *Landerer and Swenson* [2012] with removing the atmospheric load effects. After the gridded TWS anomalies are obtained, the linear trend of TWS change is estimated with the same as GRACE.

3. Secular Variations and Analysis

3.1. Ice Thinning Rates

The total glacier-covered area on Alaska is 86,715 km^2, which is provided by a new glacier inventory (Randolph Glacier Inventory version 2.0) derived from satellite imagery [*Pfeffer et al*., 2014]. Alaska has the greatest amount of glacier area of all global mountain glacier regions, which contains glaciers with rapid rates of mass loss affected by the climatic change. The Alaskan glaciers are characterized by the heterogeneous behavior of the ice thickness change rates in Figure 3. Because the temperature and precipitation vary with the elevation change, the glacier change rates have strong correlation with the elevation measured by ICESat over the period from 2003 to 2009. The ice thickness thinning rates are 2–4 m/yr at low elevations and close to zero at high elevations. The fast rate changes are occurring at the Malaspina and Bering glaciers. The general tendency of ice thinning implies that most of the Alaskan glaciers are not in dynamic equilibrium, while the surface mass balance has been affected by the glacier melting. The surface melting dominated the

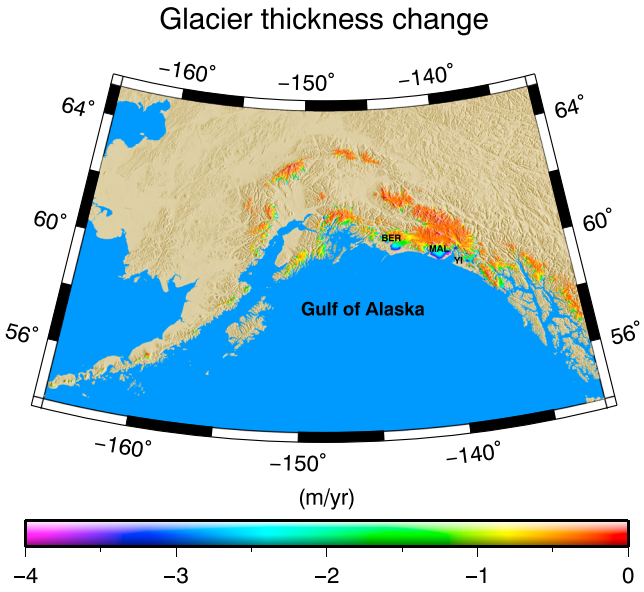

Figure 3. The ice thinning rates of Alaska glaciers measured by ICESat from 2003 to 2009.

Alaskan glacier mass balance by lidar altimetry [*Larsen et al.*, 2015]. Airborne laser altimetry measurements throughout Alaska and Canada have similar pattern of ice thickness change, but with smaller coverage [*Arendt et al.*, 2008].

Many factors, including glacier dynamics, wind drift, and measurement noise, contribute the local rates variation. The total glacier volumetric change is estimated at $-76.6\,km^3$/yr, and the uncertainties of the rates estimate will be discussed in the next section.

3.2. GPS Uplift Rates

The uplift rates are observed by 156 GPS stations in total in Alaska. The dense GPS stations provide an opportunity to make a clear image of the uplift pattern in Alaskan glaciers. To well characterize the pattern of vertical rates in Alaska, the distribution of uplift rates is interpolated by fitting a continuous, curved surface using Generic Mapping Tools (GMT) program surface [*Wessel and Smith*, 1998] in Figure 4. The vertical rates of GPS stations range from −7 mm/year to 30 mm/year, which are really tremendously great uplift on the Earth surface. Most of the GPS stations on the Alaskan glacier area are experiencing uplift, which is consistent with the general feature of contour map from *Larsen et al.* [2004] and *Larsen et al.* [2005]. The greatest uplift rates in Alaska are distributed on St. Elias Mountains and Yakutat Icefield, while the uplift peak, close to 30 mm/yr, is centered over the Yakutat Icefield.

There are two dominating factors contributing to the uplift pattern in Alaska, which are the elastic uplift caused by the current glacier melting and viscoelastic rebound following the Last Glacier Maximum and post-Little Ice Age (LIA) deglaciation [*Clark*, 1977]. On the other hand, the tectonic motion may also make a contribution to the uplift pattern but is less than 5 mm/yr in Alaska [*Larsen et al.*, 2005].

3.3. GRACE TWS Trend

The GRACE gravity RL05 solutions have been used to estimate the surface mass change on the Alaska region with 1° grid resolution. At each grid point, the trend of TWS change can be estimated by using the weighted least squares method. The long-term mass changes in Alaska measured by GRACE from 2003 to 2009 are shown in Figure 5a. A prominent glacier melting trend in the mountains range has been detected by GRACE, which indicates the significant mass loss in this region. Due to the truncation and filtering effects in processing GRACE data, the glacier mass loss signal has spread to an extensively large area with an attenuating trend. The magnitude of the mass anomaly on St. Elias Mountains is measured at about 50 mm/yr in equivalent water thickness, which is really small comparing to the magnitude measured by ICESat measurements. After the leakage effects are corrected by the forward modeling approach [*Jin and Zou*, 2015], the attenuated signals are restored in Figure 5b.

The long-term trend mainly contains the contribution of glacier melting in Alaska and GIA effects in LGM and post-LIA. It has big uncertainty to estimate the ice melting in post-LIA, which results in the difficulty to determine the nonnegligible GIA effects. Therefore, other observation data are necessary to be combined with GRACE to separate the glacier mass loss with GIA effects.

4. Density and GIA Effects

The average ice thinning rates measured by ICESat observations are on the order of ~30 cm/yr, while the uncertainty is ~3 cm/yr that is close to the magnitude of GIA effect in Alaska [*Larsen et al.*, 2005]. Moreover,

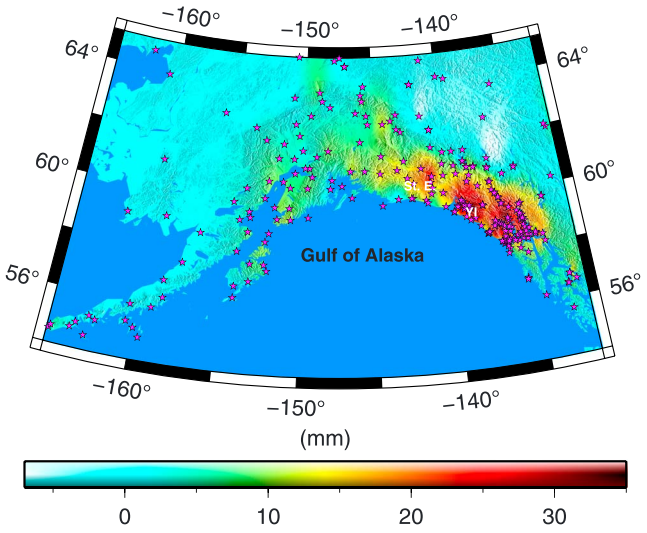

Figure 4. The uplift pattern in Alaskan region from GPS by fitting a continuous and curved surface to GPS uplift using GMT program surface.

the ICESat laser altimetry measurement is more sensitive to the ice thinning rates in Alaska. Therefore, it is assumed that the thickness change rates by ICESat measurement completely result from the glacier mass loss without consideration of GIA effects. On the other hand, the trend of surface total water from Global Land Data Assimilation System (GLDAS)/Noah is obtained for non-glacier area. Both glacier mass loss and GIA effects contribute to the uplift measured by GPS vertical displacement and TWS trend derived by GRACE gravity. Here a method in estimating the average density of the glaciers is proposed by using ICESat, GRACE, and GPS measurements:

1. The average density of the mountain glaciers is assumed to be from 400 kg/m^3 to 900 kg/m^3 [*Cox and March*, 2004; *Cuffey and Paterson*, 2010; *Huss*, 2013]. The glacier mass loss rates are estimated by converting the ice thinning rates from ICESat measurements for different values of the average density. The value of average density increases with a step of 10 kg/m^3 from 400 kg/m^3 to 900 kg/m^3.
2. Based on the results of the first step, the glacier mass change rates are estimated. The elastic uplifts caused by the glacier mass loss on each GPS stations are computed by the method of *Farrell* [1972], in which the glacier mass loads are convolved with Green's function over the glaciers masses. The spherical harmonic order of Green's function is truncated up to 500 in this study, which is accurate enough to compute the elastic uplift. The GIA effects of LGM and LIA for all GPS stations are estimated by subtracting the elastic uplifts from the vertical rates of all GPS stations.
3. To be consistent with the processing strategy of GRACE measurement, mass rates from glacier mass loss and surface total water change of GLDAS are converted into fully normalized spherical harmonic (SH) coefficients of up to degree and order 60. The monthly gravity coefficients of GRACE RL05 from 2003 to 2009 are fitted for all 60 degrees and orders, and the rates of each degree and order are obtained in this study. The SH coefficients of mass rates are subtracted from the rates of SH coefficients from GRACE for each degree and order. Therefore, the residual SH coefficients are used to estimate the GIA effects in Alaska with the method proposed by *Purcell et al*. [2011]. In order to reduce the leakage errors in estimating the GIA uplift rates, the forward modeling method [*Jin and Zou*, 2015] has been used in this study.
4. The GIA effects at each GPS station and gridded GIA uplift from GRACE in steps 2 and 3 are estimated, respectively. The misfits of GIA effects from GPS with GRACE are computed by the interpolation of gridded GIA uplift on each GPS station. Based on the correlation and weighted root-mean-square (RMS) for each density value, the optimal average density is well determined.

4.1. Density of Glaciers

A series of assessments have been performed through the comparison of GPS- and GRACE-estimated GIA uplifts for each density value. Figure 6 shows the GIA effects from GPS and GRACE under the assumption of average density equal to 400 kg/m^3, 500 kg/m^3, 600 kg/m^3, 700 kg/m^3, 800 kg/m^3, and 900 kg/m^3, respectively. The elastic uplift rates caused by the glacier mass loss range between 0.5 mm/yr and 13 mm/yr with an assumption of average density at 900 kg/m^3. With different assumption of average density, the elastic uplift rates are directly proportional to the rates from average density at 900 kg/m^3. The elastic uplift rates are determined by the ice thinning rates measured from ICESat. The uncertainties of measurements will be discussed in the next section. When the glacier mass loss signals measured by ICESat are subtracted from

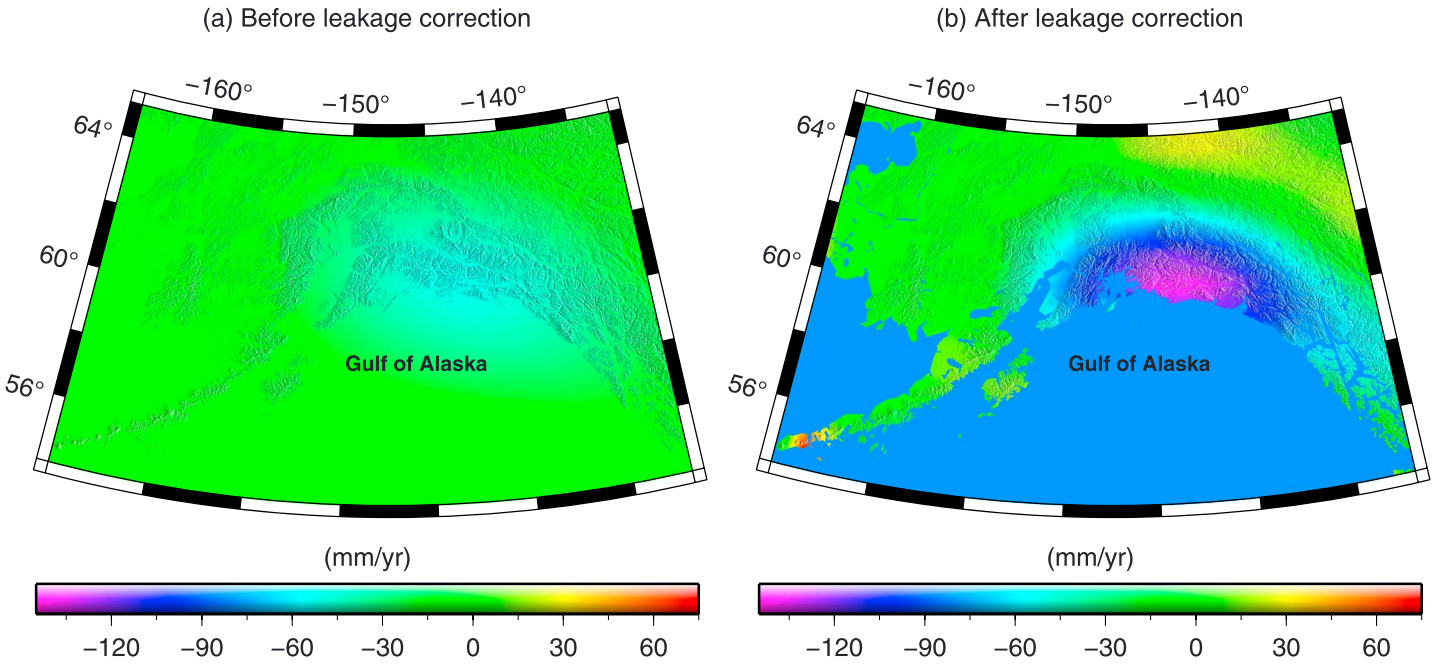

Figure 5. The trends of TWS change measured by GRACE from 2003 to 2009 (a) before leakage correction and (b) after correction using forward modeling method.

GRACE, the residual signal is generally assumed to be caused by GIA effects. For small values of average density, like 400–500 kg/m^3, the negative GIA uplift from GRACE on the central Alaska mountain can be observed in Figures 6a and 6b, which are not consistent with results from GPS. The negative signal of GIA uplift in central Alaska corresponding to low average density is contrary to the modeling result by *Larsen et al.* [2005] and difficult to be explained by GPS measurements. The pattern and magnitude of GIA vertical uplift from GRACE significantly depend on the determination of average density. The obvious disagreement between GPS- and GRACE-induced uplift indicates the inappropriate assumption of average density. As the average density increases from Figures 6a to 6f, the greater positive uplift can be observed from GRACE in southeast Alaska and GIA uplift from GPS is reduced in magnitude, which is consistent with the result of *Sato et al.* [2011]. The Yakutat Icefield and Glacial Bay in southeast Alaska have suffered the largest amount of glacier mass loss during the LIA, where the dominant uplift signal has been found. The positive uplift region is visible mostly in southeast Alaska, along with a zone of subsidence in northeast part from GRACE. Some permissive uplifts of higher or lower values from GPS than GRACE are demonstrated in the study region, which will be discussed in the next section about uncertainties of measurements.

The extent of GIA uplift at each GPS station fitted to the gridded surface uplift by GRACE determines the choice of optimal average density. Theoretically speaking, the GIA uplift rates derived from GRACE can explain the uplift rates at GPS stations and have good consistency with each other when the optimal average density is appropriately assumed. Due to the limitation and uncertainties of each measurement, the differences within tolerance are obtained for different choices of average density. Figures 7 and 8 provide the correlations and difference of GPS-induced uplift and GRACE-induced uplift for every choice of average density corresponding to Figure 6. The average GPS-induced uplift shows greater magnitude than GRACE in Figure 7a, which also indicates low correlation between them. It is conformed to the facts that the correlation increases when the average density is gradually close to the optimal density. The difference between GPS- and GRACE-induced uplift rates are plotted as histograms in Figure 8, which shows the distribution of all differences at each GPS station. If the differences are assumed to follow the normal distribution, the average value of the difference should be close to zero, which has been illustrated in Figures 8d and 8e. When quantifying the difference between GPS- and GRACE-induced uplift rates, it is necessary to consider the error-weighted difference with different assumptions of average density. The correlation and weighted RMS with different average densities are estimated, which are used to determine the optimal average density value. The results in Figure 9 show that the average density of 750 kg/m^3 is the optimal value for the glaciers of Alaska. By

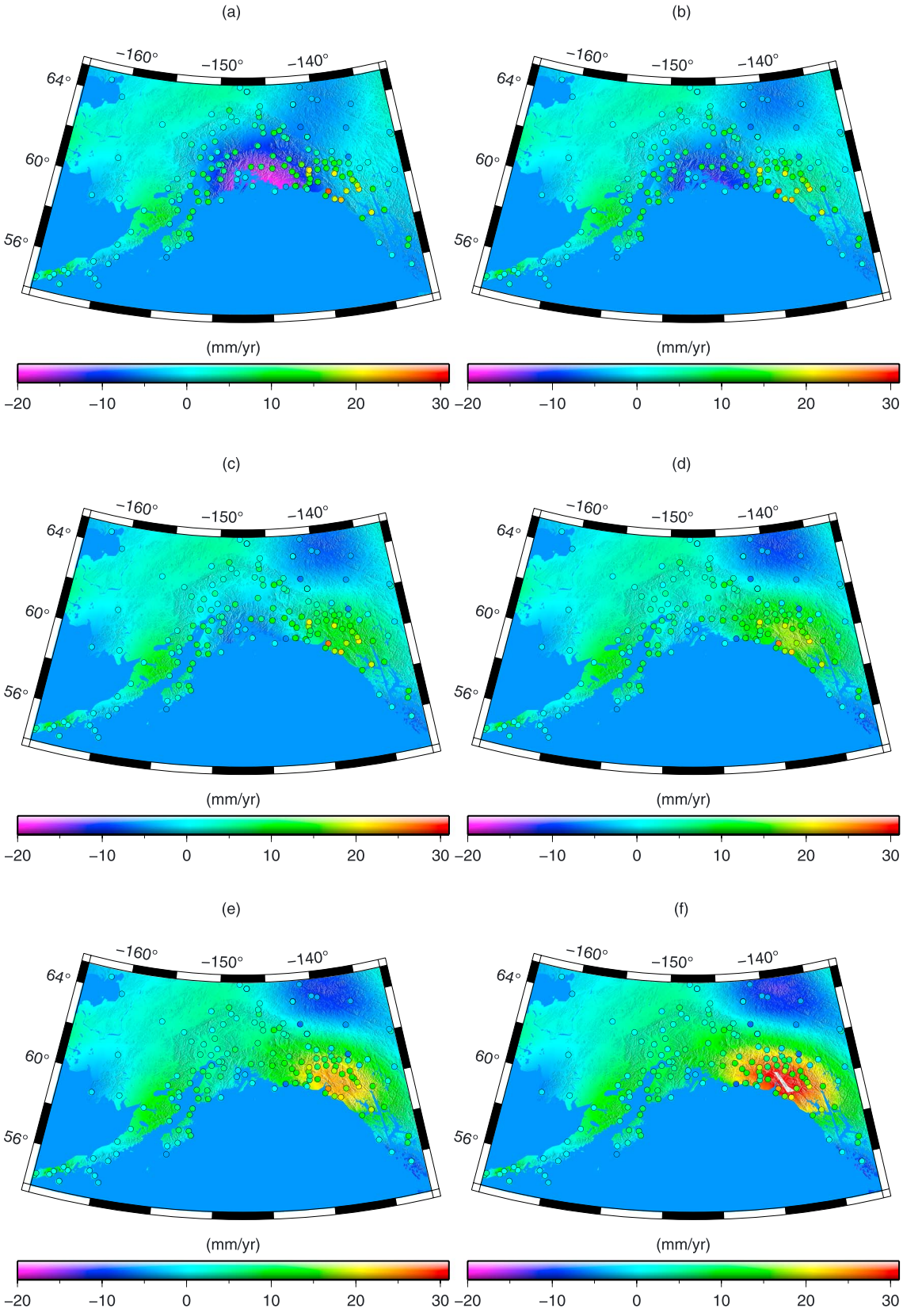

Figure 6. Viscous-only GIA uplift rates determined from GPS observations (circles) and the residual GRACE signal (shading) after removing mass changes due to glaciers and terrestrial hydrology with the average density of (a) 400 kg/m^3, (b) 500 kg/m^3, (c) 600 kg/m^3, (d) 700 kg/m^3, (e) 800 kg/m^3, (f) and 900 kg/m^3.

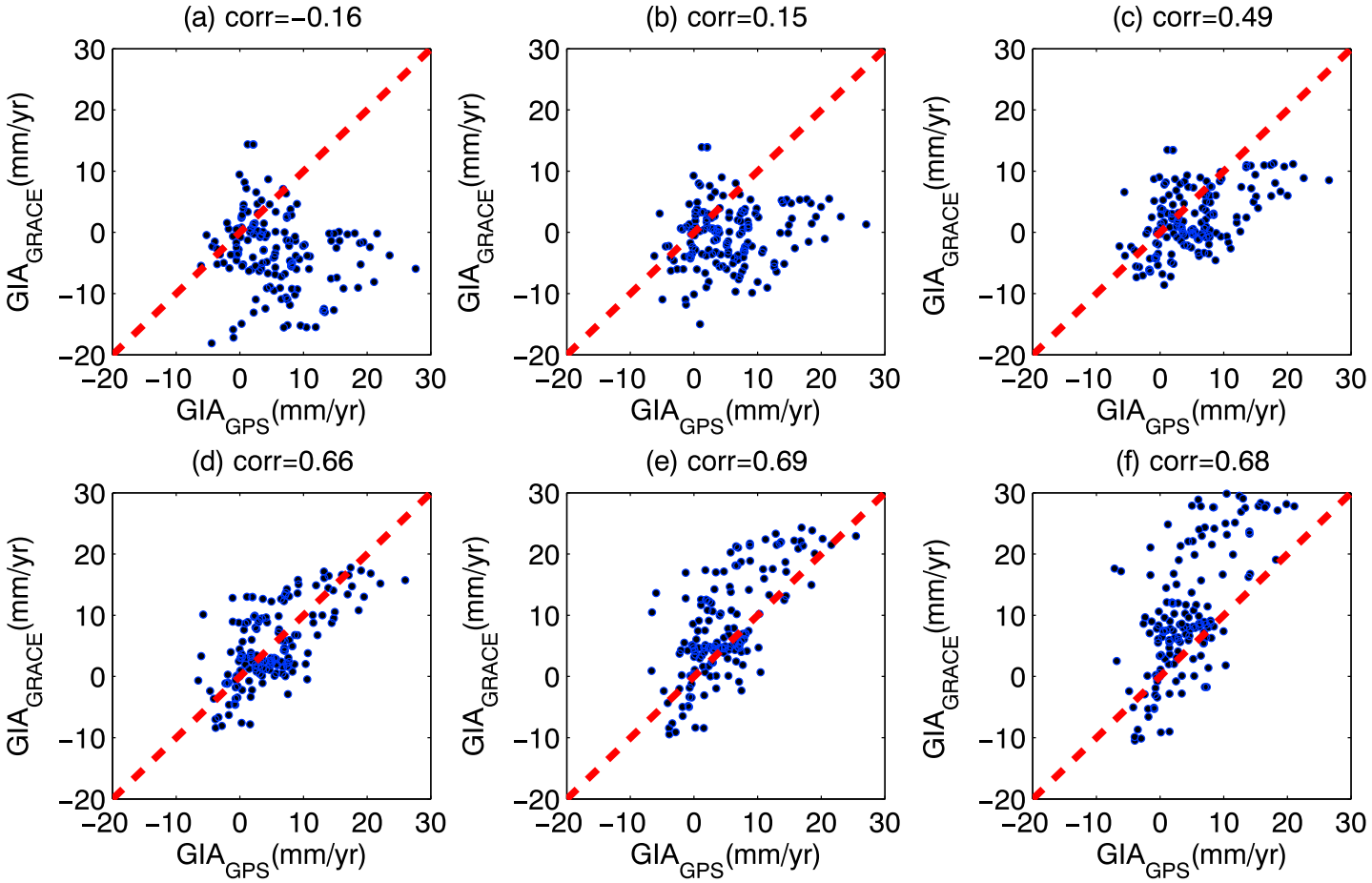

Figure 7. The scatterplots and correlations of GPS and GRACE induced uplift rates in different average densities.

converting the volumetric change measured by ICESat to mass loss, the corresponding glacier mass loss would be −57.5 Gt/yr for the whole region.

The Alaskan glaciers have a total volume of 20,400 km^3 with an average thickness of 226 m for the whole region [*Huss and Farinotti*, 2012]. When the average density of the Alaskan glaciers is estimated, it is possible to construct the depth-density profile. The typical density from snow to ice can be obtained [*Cuffey and Paterson*, 2010] as (1) damp new snow (100–200 kg/m^3), (2) settled snow (200–300 kg/m^3), (3) wind packed snow (350–400 kg/m^3), (4) firn (400–830 kg/m^3), and (5) glacier ice (830–917 kg/m^3). Figure 10 shows the depth-density profiles with different average densities based on the empirical depth-density relationship [*Arthern et al.*, 2013]. The depth-density profiles show glacial density variation information with depths in Alaska. No differences are found at the top three layers in different average densities, whose depths are 3.3m, 7.0m and 11.4m from the surface. The four-layer ranges from 11.4m to 130m and the five-layer is from 130m to the bottom. The five-layer model is well simplifying the depth-density relation, which characterizes the profile of glaciers in Alaska based on the empirical equation.

4.2. GIA Estimation in Alaska

The great uplift pattern has been demonstrated in Alaska, but the elastic uplift of glacier melting contributes only about 40% of the observed uplift. Another significant portion of the uplift can be explained by the GIA effects. The ongoing isostatic rebound from LGM has been computed with ICE-6G model by *Peltier et al.* [2015], but the uplift of GIA effects from LGM is very small comparing to the uplift signal in Alaska. The GIA effects of LGM in Alaska are also checked by *Sato et al.* [2011] with a modified four-layer Earth model, which shows the effects on the order of 1–2 mm/yr. Therefore, the isostatic uplift in Alaska from LIA plays important

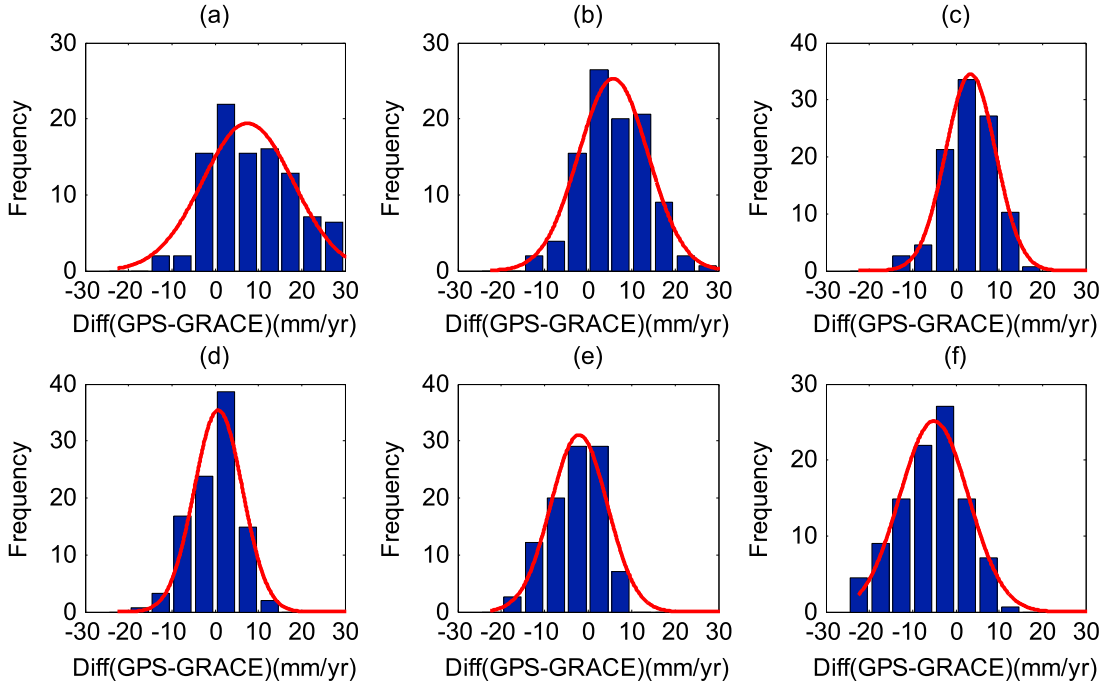

Figure 8. The histograms of the differences between GPS and GRACE uplift rates in different average densities. The red lines show the curves fitted to a Gaussian distribution for all differences.

role in the regional uplift pattern. The LIA glaciation begins from 1200 A.D. and reaches its greatest extent at 1900 A.D. in Alaska [*Wiles et al*., 1999; *Calkin et al*., 2001]. The accurate modeling of the isostatic uplift from LIA relies on the sufficient knowledge of the ice load model and Earth model. Based on the previous work constraining the timing of advance and retreat of the Alaskan glacier [*Wiles et al*., 1999; *Calkin et al*., 2001], *Larsen et al*. [2004] has developed ice load model estimating the regional volume change of the last 2 kyr history. A regional load model combining with a separated load for Glacial Bay has been applied in modeling the isostatic rebound effects. The ice load history of the glacier volume change and the ice load model of Alaskan glaciers could be found in *Larsen et al*. [2004].

The ice load model and ice load history were taken as input for the code "TABOO" developed by *Spada* [2003] and *Spada et al*. [2003]. In order to model the viscous component of the response from LIA, different kinds of Earth models with various viscous parameters are tested to search for optimum fit with measurements. A thin, low viscosity asthenosphere overlaying the upper mantle was proposed as part of the Earth model in previous studies [*Larsen et al*., 2005; *Sato et al*., 2011; *Hu and Freymueller*, 2012]. The thickness of elastic lithosphere and the asthenosphere is assumed to be 60 km and 110 km, which is consistent with previous studies. The viscosity of the asthenosphere is an unknown parameter, which will be determined by the misfits of the modeling uplift rates and measurements. The standard reduced chi-square χ^2 will be adopted in order to compare the fit to the models as follows:

$$\chi^2 = \sum_{i=1}^{n} \frac{\left(h_i^O - h_i^M\right)^2}{{\sigma^2}_i} / f \tag{5}$$

where h_i^O and h_i^M are the ith observation and corresponding modeling value, respectively; σ_i is the uncertainty of the ith observation; f is the degrees of freedom; and n is the number of data.

The optimal density of glacial volume change in Alaska has been estimated as 750 kg/m^3, so the elastic uplift rates caused by the ice mass loss can be accurately subtracted from GPS uplift rates and GRACE TWS trend. The GIA uplift rates measured by GPS and GRACE are the observation data for fitting the optimal GIA model in Figure 11. The model predictions are compared with observation data when we change the viscous parameters. The best fit model consists of a 60 km elastic lithosphere and 110 km thick asthenosphere with

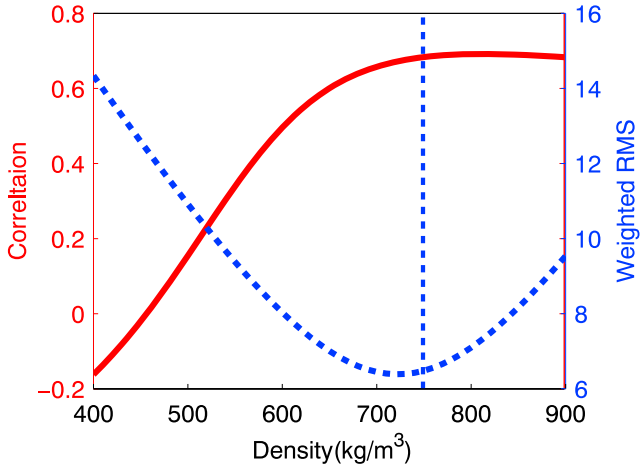

Figure 9. The correlations and weighted RMS under the assumption of different average densities.

a viscosity of 2.0×10^{19} Pa s, which is consistent with *Larsen et al*. [2004]. The contour of the modeling results shows good consistency with observation data in Alaska mountain area in Figure 11. The negative signal in northeast part of Alaska derived from GRACE cannot well be explained by the model prediction because of loose constraint in GIA model for the nonglacier area. It is possible that the "true" TWS trend in northeast part is not well modeled in GLDAS model, while to thus exist in the GIA uplift of GRACE.

4.3. Uncertainties and Discussions

The uplift rates measured by GPS sites include continuous observations and campaign observations, whose uncertainties depend on the observation time period of successive measurements. The mean uncertainties of 101 continuous GPS observations and 55 campaign observations are 0.5 mm/yr and 2.8 mm/yr, respectively. The accuracy of continuous GPS observations is better than the campaign observation, but most of the continuous GPS observations are located at the western part of Alaska. The uncertainties include the error due to the reference frame [*Argus*, 2007], but they only represent less than 10% of the observed uplift rates. Another contribution to the total uplift rates could arise from tectonic motion, which is not taken into consideration here. It has been discussed by *Larsen et al*. [2005] that the largest tectonic contribution of the uplift rates would be less than 5 mm/yr, and it is difficult to quantify the tectonic uplift at every GPS station.

The ice thinning rates measured by ICESat are determined by campaign observations, which are associated with uncertainties in determination of the surface slope and temporal sampling of nonlinear elevation

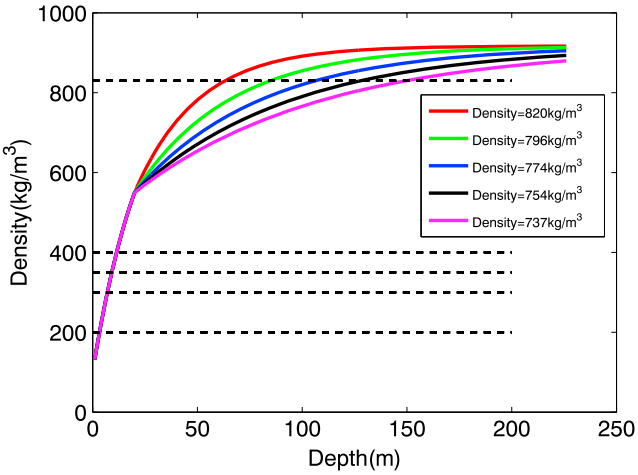

Figure 10. The depth-density profiles for different average densities.

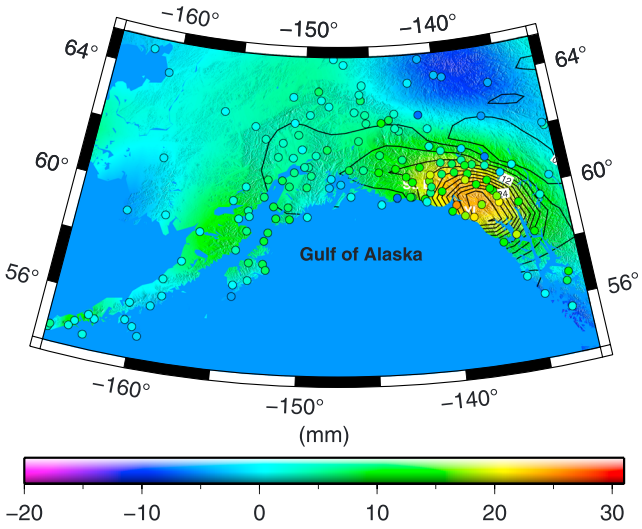

Figure 11. The best model predicted uplift rates by fitting the observation data, which are shown in contour lines.

changes. A plane fitting method has been applied in processing the ICESat measurements, and the precisions of elevation change *dh*/*dt* on each plane can be determined. Because there is enough sampling of *dh*/*dt* for all the elevation change, the uncertainties of volumetric change estimation can be reduced by spatial extrapolation of *dh*/*dt*, where the polynomial fitting method is used. An area-averaged elevation change error was introduced to estimate the standard error as follows:

$$\varepsilon = \frac{\sigma_{\text{fit}}}{\sqrt{N-4}} \tag{6}$$

where σ_{fit} is the RMS error of the polynomial fit and N is the number of all uncorrelated observations in the region. The correlation length is assumed to be 5 km in Alaska [*Arendt et al*., 2013]. The standard error of 0.04 m/yr for the area-averaged *dh*/*dt*, and the uncertainty of the volumetric change in Alaska is 8.6 km^3/yr.

The GRACE TWS rates have been obtained in Alaska from the least squares fit, and the errors are also estimated for all grid points. The mean ratios between gridded GRACE TWS and errors will be approximated as the percentages between formal errors and GRACE TWS after forward modeling. More information can be seen in *Jin and Zou* [2015]. Before correcting the glacier mass signal measured by ICESat for GRACE TWS rates, the rates for all degree and order coefficients associated with the uncertainties of GRACE are also affected.

In addition, ICESat data are relatively sparse over Alaska, which will induce errors by not resolving the higher spatial resolution changes when linking the ICESat observations to the Earth model simulations, while Airborne Altimetry is able to capture a greater amount of the spatial variability than the ICESat data [*Larsen et al*., 2015]. In the future, NASA airborne altimetry observations will be further used to estimate glacial density model in Alaska.

Furthermore, the density profile has some uncertainty for Alaska glaciers and the correction factor for the density of geodetic volume change and other changes under different scenarios as well as the presence of liquid water in the firn also affect results [*Huss*, 2013], which should be further considered in the future for Alaska glacier density estimation.

5. Conclusions

The Alaska glaciers are experiencing tremendous mass loss recently, which are underestimated by the constraint of the space geodetic measurements. The uplift rates measured by GPS stations in Alaska show great uplifts, which include the contribution of elastic uplift caused by glacier mass loss and the viscous component of response by glacier mass loss during LIA. The campaign observations by ICESat measurements from 2003 to 2009 are available to constrain the ice thinning rates of Alaska glaciers, which provide a preliminary estimate of volumetric change at -76.6 ± 8.6 km^3/yr. The GRACE has shown great ability to

detect the negative long-term trend of TWS in Alaska, which is also contaminated by the GIA effects. Based on the measurements of GPS, ICESat, and GRACE, the optimal average density of the Alaskan glaciers has been estimated by separating glacier mass loss signal with GIA effects. The glacier mass loss measured by ICESat depends on the average density, which is subtracted from GPS uplift rates and TWS trends of GRACE. The optimal average density is determined as 750 kg/m^3, and the corresponding glacier mass loss would be -57.5 ± 6.5Gt. Based on the empirical depth-density relationship, the depth-density profiles are constructed, which provide the knowledge of depth dependent glacier density profile in Alaska.

After correcting the glacier mass loss signal for GPS uplift rates and GRACE measurements, the best model for the GIA effects during LIA in Alaska is obtained by fitting the model uplift rates with GPS and GRACE residual signals. A low-viscosity asthenosphere is invoked in the viscous structure in the Earth model. The best fitting model consists of a 60 km elastic lithosphere and 110 km thick asthenosphere with a viscosity of 2.0×10^{19} Pa s over a two-layer mantle. The largest uplift rate of GIA effects is located at Glacier Bay.

Acknowledgments
The authors are grateful to UNAVCO Plate Boundary Observatory and NASA MEaSUREs projects for GPS data and the National Snow and Ice Data Center for ICESat data. The GPS products used in this study are available at ftp://sideshow.jpl.nasa.gov/pub. We also thank those who made GRACE observations available. The figures in this paper were generated by using the Generic Mapping Tools (GMT) software [*Wessel and Smith*, 1998]. This research is supported by the National Natural Science Foundation of China (NSFC) Project (grant 11373059).

References

Arendt, A. A., S. B. Luthcke, C. F. Larsen, W. Abdalati, W. B. Krabill, and M. J. Beedle (2008), Validation of high-resolution GRACE mascon estimates of glacier mass changes in the St Elias Mountains, Alaska, USA, using aircraft laser altimetry, *J. Glaciol.*, *54*(188), 778–787, doi:10.3189/002214308787780067.

Arendt, A., et al. (2012), Randolph Glacier Inventory (RGI), Vers. 1.0: A dataset of global glacier outlines, Global Land Ice Measurements from Space, Boulder, Colo., Digital media. [Available at http://www.glims.org/RGI/randolph.html.]

Arendt, A., S. Luthcke, A. Gardner, S. O'Neel, D. Hill, G. Moholdt, and W. Abdalati (2013), Analysis of a GRACE global mascon solution for Gulf of Alaska Glaciers, *J. Glaciol.*, *59*(217), 913–924, doi:10.3189/2013JoG12J197.

Argus, D. (2007), Defi ning the translational velocity of the reference frame of Earth, *Geophys. J. Int.*, *169*, 830–838, doi:10.1111/j.1365-246X.2007.03344.

Argus, D., M. B. Heflin, G. Peltzer, F. Crampe, and F. H. Webb (2005), Interseismic strain accumulation and anthropogenic motion in metropolitan Los Angeles, *J. Geophys. Res.*, *110*, B04401, doi:10.1029/2003JB002934.

Arthern, R. J., H. F. J. Corr, F. Gillet-Chaulet, R. L. Hawley, and E. M. Morris (2013), Inversion for the density-depth profile of polar firn using a stepped-frequency radar, *J. Geophys. Res. Earth Surf.*, *118*, 1257–1263, doi:10.1002/jgrf.20089.

Avsar, N., S. G. Jin, H. Kutoglu, and G. Gurbuz (2016), Sea level change along the Black Sea coast from satellite altimetry, tide gauge and GPS observations, *Geod. Geodyn.*, *7*(1), 50–55, doi:10.1016/j.geog.2016.03.005.

Bader, H. (1954), Sorge's law of densification of snow on high polar glaciers, *J. Glaciol.*, *2*(15), 319–323.

Beamer, J., D. Hill, A. Arendt, and G. Liston (2016), High-resolution modeling of coastal freshwater discharge and glacier mass balance in the Gulf of Alaska Watershed, *Water Resour. Res.*, *52*(5), 3888–3909, doi:10.1002/2015WR018457.

Bevis, M., and A. Brown (2014), Trajectory models and reference frames for crustal motion geodesy, *J. Geod.*, *88*, 283–311, doi:10.1007/s00190-013-0685-5.

Bevis, M., J. Wahr, S. A. Khan, F. B. Madsen, A. Brown, M. Willis, E. Kendrick, P. Knudsen, J. E. Box, and T. van Dam (2012), Bedrock displacements in Greenland manifest ice mass variations, climate cycles, and climate change, *Proc. Natl. Acad. Sci. U.S.A.*, *109*, 11,944–11,948, doi:10.1073/pnas.1204664109.

Bhang, K. J., F. W. Schwartz, and A. Braun (2007), Verification of the vertical error in C-band SRTM DEM using ICESat and Landsat-7, Otter Tail County, MN, *IEEE Trans. Geosci. Remote Sens.*, *45*, 36–44.

Borsa, A. A., G. Moholdt, H. A. Fricker, and K. M. Brunt (2013), A range correction for ICESat and its potential impact on ice-sheet mass balance studies, *Cryosphere*, *8*, doi:10.5194/tc-8-1-2014.

Calkin, P. E., G. C. Wiles, and D. J. Barclay (2001), Holocene coastal glaciation of Alaska, *Quat. Sci. Rev.*, *20*, 449–461.

Chen, J. L., B. D. Tapley, and C. R. Wilson (2006), Alaskan mountain glacial melting observed by satellite gravimetry, *Earth Planet. Sci. Lett.*, *248*(1–2), 368–378.

Cheng, M., and B. D. Tapley (2004), Variations in the Earth's oblateness during the past 28 years, *J. Geophys. Res.*, *109*, B09402, doi:10.1029/2004JB003028.

Clark, J. A. (1977), An inverse problem in glacial geology: The reconstruction of glacier thinning in Glacier Bay, Alaska between A.D. 1910 and 1960 from relative sea-level data, *J. Glaciol.*, *18*, 481–503.

Compton, K., R. A. Bennett, and S. Hreinsdóttir (2015), Climate-driven vertical acceleration of Icelandic crust measured by continuous GPS geodesy, *Geophys. Res. Lett.*, *42*, 743–750, doi:10.1002/2014GL062446.

Cox, L. H., and L. S. March (2004), Comparison of geodetic and glaciological mass-balance techniques, Gulkana Glacier, Alaska, USA, *J. Glaciol.*, *50*, 63–70.

Cuffey, K. M., and W. S. B. Paterson (2010), *The Physics of Glaciers*, pp. 704, Butterworth-Heinemann, Oxford.

Farrell, W. E. (1972), Deformation of the Earth by surface loads, *Rev. Geophys. Space Phys.*, *10*, 761–797.

Fu, Y., J. T. Freymueller, and T. Jensen (2012), Seasonal hydrological loading in southern Alaska observed by GPS and GRACE, *Geophys. Res. Lett.*, *39*, L15310, doi:10.1029/2012GL052453.

Hassan, A., and S. G. Jin (2016), Water storage changes and balances in Africa observed by satellite gravimetry and hydrologic models, *Geod. Geodyn.*, *7*(1), 39–49, doi:10.1016/j.geog.2016.03.002.

Howat, I. M., B. E. Smith, I. Joughin, and T. A. Scambos (2008), Rates of southeast Greenland ice volume loss from combined ICESat and ASTER observations, *Geophys. Res. Lett.*, *35*, L17505, doi:10.1029/2008GL034496.

Hu, Y., and J. T. Freymueller (2012), Geodetic observations of glacial isostatic adjustment in Southeast Alaska and its implication of Earth rheology Abstract G21A-0872 presented at 2012 Fall Meeting, AGU, San Francisco, Calif.

Huss, M. (2013), Density assumptions for converting geodetic glacier volume change to mass change, *Cryosphere*, *7*(3), 877–887, doi:10.5194/tc-7-877-2013.

Huss, M., and D. Farinotti (2012), Distributed ice thickness and volume of all glaciers around the globe, *J. Geophys. Res.*, *117*, F04010, doi:10.1029/2012JF002523.

Jiang, Y., T. H. Dixon, and S. Wdowinski (2010), Accelerating uplift in the North Atlantic region as an indicator of ice loss, *Nat. Geosci.*, *3*, 404–407, doi:10.1038/ngeo845.

Jin, S. G., and F. Zou (2015), Re-estimation of glacier mass loss in Greenland from GRACE with correction of land-ocean leakage effects, *Global Planet. Change*, *135*, 170–178, doi:10.1016/j.gloplacha.2015.11.002.

Jin, S. G., and G. P. Feng (2013), Large-scale variations of global groundwater from satellite gravimetry and hydrological models, 2002–2012, *Global Planet. Change*, *106*, 20–30, doi:10.1016/j.gloplacha.2013.02.008.

Jin, S. G., and G. P. Feng (2016), Uncertainty of GRACE-estimated land water and glaciers contributions to sea level change during 2003-2012, in *Proceeding of IEEE International Geoscience and Remote Sensing Symposium*, pp. 6189–6192, IGARSS, Beijing, doi:10.1109/IGARSS.2016.7730617.

Jin, S. G., and P. H. Park (2006), Strain accumulation in South Korea inferred from GPS measurements, *Earth Planets Space*, *58*(5), 529–534, doi:10.1186/BF03351950.

Jin, S. G., L. J. Zhang, and B. D. Tapley (2011), The understanding of length-of-day variations from satellite gravity and laser ranging measurements, *Geophys. J. Int.*, *184*(2), 651–660, doi:10.1111/j.1365-246X.2010.04869.x.

Jin, S. G., A. A. Hassan, and G. P. Feng (2012), Assessment of terrestrial water contributions to polar motion from GRACE and hydrological models, *J. Geodyn.*, *62*, 40–48, doi:10.1016/j.jog.2012.01.009.

Jin, S. G., T. van Dam, and S. Wdowinski (2013), Observing and understanding the Earth system variations from space geodesy, *J. Geodyn.*, *72*, 1–10, doi:10.1016/j.jog.2013.08.001.

Ke, L., X. Ding, and C. Song (2015), Heterogeneous changes of glaciers over the western Kunlun Mountains based on ICESat and Landsat-8 derived glacier inventory, *Remote Sens. Environ.*, *168*, 13–23.

Landerer, F. W., and S. C. Swenson (2012), Accuracy of scaled GRACE terrestrial water storage estimates, *Water Resour. Res.*, *48*, W04531, doi:10.1029/2011WR011453.

Larsen, C. F., R. J. Motyka, J. T. Freymueller, K. A. Echelmeyer, and E. R. Ivins (2004), Rapid uplift of southern Alaska caused by recent ice loss, *Geophys. J. Int.*, *158*, 1118–1133.

Larsen, C. F., R. J. Motyka, J. T. Freymuller, K. A. Echelmeyer, and E. R. Ivins (2005), Rapid viscoelastic uplift southern Alaska caused by post-Little Ice Age glacial retreat, *Earth Planet. Sci. Lett.*, *237*, 548–560.

Larsen, C. F., R. J. Motyka, A. A. Arendt, K. A. Echelmeyer, and P. E. Geissler (2007), Glacier changes in southeast Alaska and northwest British Columbia and contribution to sea level rise, *J. Geophys. Res.*, *112*, F01007, doi:10.1029/2006JF000586.

Larsen, C. F., E. Burgess, A. A. Arendt, S. O'Neel, A. J. Johnson, and C. Kienholz (2015), Surface melt dominates Alaska glacier mass balance, *Geophys. Res. Lett.*, *42*, 5902–5908, doi:10.1002/2015GL064349.

Luthcke, S. B., A. A. Arendt, D. D. Rowlands, J. J. McCarthy, and C. F. Larsen (2008), Recent glacier mass changes in the Gulf of Alaska region from GRACE mascon solutions, *J. Glaciol.*, *54*(188), 767–777, doi:10.3189/002214308787779933.

Marechal, A., S. Mazzotti, J. L. Elliott, J. T. Freymueller, and M. Schmidt (2015), Indentor-corner tectonics in the Yakutat-St. Elias collision constrained by GPS, *J. Geophys. Res. Solid Earth*, *120*, 3897–3908, doi:10.1002/2014JB011842.

Milne, G. A., J. L. Davis, J. X. Mitrovica, H.-G. Scherneck, J. M. Johansson, M. Vermeer, and H. Koivula (2001), Space-geodetic constraints on glacial isostatic adjustment in Fennoscandia, *Science*, *291*, 2381–2385, doi:10.1126/science.1057022.

Moholdt, G., C. Nuth, J. O. Hagen, and J. Kohler (2010), Recent elevation changes of Svalbard glaciers derived from ICESat laser altimetry, *Remote Sens. Environ.*, *114*(11), 2756–2767, doi:10.1016/j.rse.2010.06.008.

Moholdt, G., B. Wouters, and A. S. Gardner (2012), Recent mass changes of glaciers in the Russian High Arctic, *Geophys. Res. Lett.*, *39*, L10502, doi:10.1029/2012GL051466.

Peltier, W. R., D. F. Argus, and R. Drummond (2015), Space geodesy constrains ice age terminal deglaciation: The global ICE-6G_C (VM5a) model, *J. Geophys. Res. Solid Earth*, *120*, 450–487, doi:10.1002/2014JB011176.

Pfeffer, W. T., A. A. Arendt, A. Bliss, et al. (2014), The Randolph Glacier Inventory: A globally complete inventory of glaciers, *J. Glaciol.*, *60*(221), 537–552, doi:10.3189/2014jog13j176.

Purcell, A., A. Dehecq, P. Tregoning, E.-K. Potter, S. C. McClusky, and K. Lambeck (2011), Relationship between glacial isostatic adjustment and gravity perturbations observed by GRACE, *Geophys. Res. Lett.*, *38*, L18305, doi:10.1029/2011GL048624.

Rignot, E., I. Velicogna, M. R. van den Broeke, A. Monaghan, and J. Lenaerts (2011), Acceleration of the contribution of the Greenland and Antarctic ice sheets to sea level rise, *Geophys. Res. Lett.*, *38*, L05503, doi:10.1029/2011GL046583.

Sato, T., C. F. Larsen, S. Miura, Y. Ohta, H. Fujimoto, W. Sun, R. J. Motyka, and J. T. Freymuller (2011), Reevaluation of the viscoelastic and elastic responses to the past and present-day ice changes in Southeast Alaska, *Tectonophysics*, *511*, 79–88, doi:10.1016/j.tecto.2010.05.009.

Shuman, C. A., H. J. Zwally, B. E. Schutz, A. C. Brenner, J. P. DiMarzio, V. P. Suchdeo, and H. A. Fricker (2006), ICESat Antarctic elevation data: Preliminary precision and accuracy assessment, *Geophys. Res. Lett.*, *33*, L07501, doi:10.1029/2005GL025227.

Spada, G. (2003), The Theory Behind TABOO Samizdat Press, Golden-White River Junction.

Spada, G., et al. (2003), TABOO, User Guide Samizdat Press, Golden-White River Junction.

Swenson, S. C., and J. Wahr (2006), Post-processing removal of correlated errors in GRACE data, *Geophys. Res. Lett.*, *33*, L08402, doi:10.1029/2005GL025285.

Swenson, S. C., D. Chambers, and J. Wahr (2008), Estimating geocenter variations from a combination of GRACE and ocean model output, *J. Geophys. Res.*, *113*, B08410, doi:10.1029/2007JB005338.

Tapley, B. D., S. Bettadpur, M. Watkins, and C. Reigber (2004), The gravity recovery and climate experiment: Mission overview and early results, *Geophys. Res. Lett.*, *31*, L09607, doi:10.1029/2004GL019920.

Van Dam, T. (2010), NCEP derived 6 hourly, global surface displacements at 2.5 × 2.5 degree spacing. [Available at http://geophy.uni.lu/ncep-loading.html.]

Velicogna, I., and J. Wahr (2002), A method for separating Antarctic postglacial rebound and ice mass balance using future ICESat Geoscience Laser Altimeter System, Gravity Recovery and Climate Experiment, and GPS satellite data, *J. Geophys. Res.*, *107*(B10), 2263, doi:10.1029/2001JB000708.

Velicogna, I., and J. Wahr (2005), Greenland mass balance from GRACE, *Geophys. Res. Lett.*, *32*, L18505, doi:10.1029/2005GL023955.

Velicogna, I., T. C. Sutterley, and M. R. van den Broeke (2014), Regional acceleration in ice mass loss from Greenland and Antarctica using GRACE time-variable gravity data, *J. Geophys. Res. Space Physics*, *41*, 8130–8137, doi:10.1002/2014GL061052.

Wahr, J., S. Swenson, V. Zlotnicki, and I. Velicogna (2004), Time-variable gravity from GRACE: First results, *Geophys. Res. Lett.*, *31*, L11501, doi:10.1029/2004GL019779.

Wessel, P., and W. H. F. Smith (1998), New, improved version of generic mapping tools released, *Eos Trans. AGU*, *79*(47), 579, doi:10.1029/98EO00426.

Wiles, G. C., D. J. Barclay, and P. E. Calkin (1999), Tree-ring-dated Little Ice Age histories of maritime glaciers from western Prince William Sound, Alaska, *Holocene*, *9*, 163–173.

Yang, Q., S. Wdowinski, and T. H. Dixon (2013), Annual variation of coastal uplift in Greenland as an indicator of variable and accelerating ice mass loss, *Geochem. Geophys. Geosyst.*, *14*, 1569–1589, doi:10.1002/ggge.20089.

Zhou, Y., S. G. Jin, R. Tenzer, and J. Feng (2016), Water storage variations in the Poyang Lake basin estimated from GRACE and Satellite Altimetry, *Geod. Geodyn.*, *7*(2), 108–116, doi:10.1016/j.geog.2016.04.003.

Zwally, H. J., et al. (2002), ICESat's laser measurements of polar ice, atmosphere, ocean, and land, *J. Geodyn.*, *34*, 405–445.